The International Journal of Advanced Manufacturing Technology (2018) 97:3671–3682
https://doi.org/10.1007/s00170-018-2178-4

ORIGINAL ARTICLE

Inverse determination of improved constitutive equation for cutting titanium alloy Ti-6Al-4V based on finite element analysis

Junxue Ren[1] · Ju Cai[1] · Jinhua Zhou[1,2] · Kaining Shi[1] · Xiangyu Li[1]

Received: 20 September 2017 / Accepted: 13 May 2018 / Published online: 29 May 2018

Abstract

Constitutive model plays an important role in finite element (FE) simulation of machining, especially the Johnson-Cook (J-C) model. Although many researches have completed on modifying the J-C model to improve FE simulation of cutting, the systematic determination scheme of the added coefficients is heretofore not available. Inverse identification approach presents a promising advantage on determining constitutive coefficient compared with traditional methods, such as Split Hopkinson Pressure Bar (SHPB). In this work, a new inverse method based on finite element analysis (FEA) is developed for determining added J-C coefficients. A modified J-C constitutive model (MJC) including hyperbolic tangent failure function is introduced for machining titanium alloy Ti-6Al-4V. The determination process of the added coefficients is taken as an optimization problem, where experimental cutting forces and the added J-C coefficients are considered as the optimization objectives and design variables, respectively. An FE model of orthogonal cutting titanium alloy Ti-6Al-4V is established on the Deform-2D simulation platform. The response surface method (RSM) is subsequently used to build the mapping relation of the simulated cutting forces and the added coefficients. Then, orthogonal cutting experiments are conducted to obtain the objective cutting forces. The firefly algorithm (FA) is employed to solve the optimization model for the optimal added J-C coefficients. Verification results show that the identified constitutive model has higher accuracy on predicting cutting forces compared with other models including the origin J-C model and the Calamaz's model.

Keywords Constitutive model · Titanium alloy Ti-6Al-4V · Inverse identification · Finite element analysis · Response surface method · Firefly algorithm

1 Introduction

Machining was one of the most frequently used processes for industrial workpieces. It was assessed that about 15% of the worth of mechanical components manufactured around the world comes from machining [1]. While many aeronautical materials were hard to machine during industrial processes. For example, although titanium alloy has become one of the most widely used materials among the aviation and aerospace field due to the high heat resistance, high strength, and strong corrosion resistance, it had a non-negligible problem for machining on account of its low thermal conductivity, low elastic modulus, and high chemical reactivity [2].

In order to avoid the economic and technical cost of tedious experiments, finite element analysis (FEA) is commonly taken as one of the most effective methods to investigate cutting mechanism [3]. Therefore, the FE simulation is usually employed to optimize process parameters and predict cutting performance. A barrier for FE modeling is the plastic constitutive model of titanium alloy Ti-6Al-4V at high strain, strain rate, and temperature. A plenty of empirical statistical models were proposed by previous researchers, such as the Johnson-Cook (J-C) model [4], Power law model [5], Zerilli-Armstrong (Z-A) model [6–8], and Mechanical Threshold Stress (MTS) model [9], and so on. Among these models, the J-C model is one of the most commonly used plastic constitutive models for machining [10–14] due to its suitability for modeling results and simple form. The traditional method to determine the J-C model parameters is the high-speed compression test, such as the Split Hopkinson Pressure Bar

✉ Jinhua Zhou
zhoujinhua@mail.nwpu.edu.cn

[1] School of Mechanical Engineering, Northwestern Polytechnical University, Xi'an 710072, Shaanxi, China

[2] Department of Mechanical Engineering, National University of Singapore, Singapore 117575, Singapore

(SHPB) test [15]. However, it needs lots of experiments to obtain high fitting precision, which leads to a high economic and time-consuming cost. Furthermore, another fatal flaw is the limited range of strain or strain rate. The available maximum strain and strain rate value of SHPB test are about 0.5 [1] and the order of 10^3 s^{-1} [16], respectively. Actually, the workpiece material usually experienced strain of 1 or even higher and strain rate in excessing of 10^4 s^{-1} during machining. The fitted J-C model by the SHPB test leads to a misunderstanding on the plastic behavior of titanium alloy Ti-6Al-4V, in which strain hardening was along with the whole machining process. Actually, there is obvious stress decline with the increase of strain when its value exceeded a critical value for titanium alloy Ti-6Al-4V [17, 18]. Some scholars attributed the stress drop to the dynamic recovery, recrystallization [19–22], and temperature softening effect [23]. Others considered the material failure mechanism due to microcrack and voiding in the primary shear band as the additional inducement [15, 24].

In order to reflect the changes of flow stress, numerous scholars carried out researches. Calamaz et al. [1] proposed an improved J-C model of titanium alloy Ti-6Al-4V, which includes the dynamic recrystallization. They added a new term to the original J-C equation and used the hyperbolic tangent function to capture the strain softening phenomenon. Subsequently, they made a further improvement by incorporating the temperature and strain rate effect [25, 26]. Sima and Özel [23] proposed an improved temperature-dependent flow softening J-C model. They deemed thermal softening effect was stronger than strain hardening effect and the strain rate sensitivity declined with the increase of strain. Karpat et al. [27] developed an improved material model of titanium alloy Ti-6Al-4V based on micromechanical constitutive model. They added an additional term into the existing model to reflect strain softening phenomenon, which is similar to the Calamaz's model. Then, they determined the additional parameters through single factor method. Andrade et al. [28] introduced a new term to the original J-C equation to describe the flow stress of titanium alloy Ti-6Al-4V when the temperature exceeded the recrystallization temperature. But this modified model is limited to a low strain range. Liu et al. [18] enlarged the application scope of strain range using a strain-based piecewise function. Subsequently, they [17] built another similar piecewise constitutive equation of titanium alloy Ti-6Al-4V, where they took the recrystallization temperature as the demarcation point. Researches [1] [28] showed the hyperbolic tangent function could be used to reflect the flow stress softening of titanium alloy Ti-6Al-4V. Although the J-C model was generally improved, the modified parameters of improved models did not be determined systematically. The methods of confirming modified parameters were SHPB test [18], single factor screening approach [23], simple search algorithm [15], and the nonlinear regression analysis based on Oxley's orthogonal cutting theory [29] in the previous studies. These methods were too simple to obtain the optimal parameters combination. And these methods still needed to be further improved.

Inverse approach based on FEA is a low-cost and effective way to determine modified parameters of material constitutive equation. In this paper, a reverse approach by integrating FEA with response surface method (RSM) and the firefly algorithm (FA) is proposed to determine the modified J-C constitutive parameters. The specific works are as follows. A modified flow softening model of titanium alloy Ti-6Al-4V is developed in Section 2. It considers dynamic recovery, recrystallization mechanisms, and failure mechanisms, and so on. An inverse approach is subsequently displayed. In Section 3, the RSM is used to relate the cutting forces to the modified J-C parameters. Then, FA is employed to search the optimal level of the added J-C coefficients. The orthogonal cutting experiments are conducted to verify the proposed J-C constitutive model in Section 4. Finally, it concludes with a summary of this research in Section 5.

2 Modified Johnson-Cook equation and determination procedure

The J-C constitutive model is widely used to reflect the plastic deformation behavior at high pressure and temperature, especially for machining. The original J-C equation is defined as a combination of three function proposed by Johnson and Cook (1983) [30] as shown in Eq. (1). Although it simultaneously considers the influence of strain, strain rate, and temperature on flow stress, it neglects the coupling effect.

$$\sigma = (A + B\varepsilon^n)\left[1 + C\left(\ln\left(1 + \frac{\dot{\varepsilon}}{\dot{\varepsilon}_0}\right)\right)\right]\left[1 - \left(\frac{T - T_r}{T_m - T_r}\right)^m\right] \tag{1}$$

where A, B, C, n, and m are empirical constants, which present the yield stress, hardening modulus, strain rate sensitivity, hardening factor, and thermal softening factor, respectively, σ is equivalent flow stress, ε is equivalent plastic strain, $\dot{\varepsilon}$ is equivalent strain rate, $\dot{\varepsilon}_0$ is reference strain rate, T is workpiece material temperature, T_r is room temperature, and T_m is the melting point of workpiece. The first square bracket term represents strain hardening in J-C equation. The second square bracket term shows that flow stress increases with increase of the strain rate. The last square bracket term reflects thermal softening phenomenon.

The flow stress increases with the increase of the strain [25]. As reviewed above, thermal softening, the microcrack, and dynamic recrystallization could result in the obvious flow softening during cutting. Researchers developed some improved J-C models to describe this

behavior. Among these models, the Calamaz's models are typical representative [1, 25, 26]. Calamaz took a critical strain value as the watershed between strain hardening and flow softening. In this paper, a similar MJC model is proposed based on the previous works as shown in Eq. (2).

$$\begin{cases} \sigma = \left[A + B\varepsilon^{n}\left(\frac{1}{\exp(\varepsilon^{a})}\right)\right]\left[1 + C\ln\left(\frac{\dot{\varepsilon}}{\dot{\varepsilon}_0}\right)\right]\left[1-\left(\frac{T-T_r}{T_m-T_r}\right)^{m}\right]\left[D + (1-D)\left(\tanh\left(\frac{1}{\varepsilon + P}\right)\right)^{s}\right] \\ D = 1-\left(\frac{T}{T_m}\right)^{d}, P = \left(\frac{T}{T_m}\right)^{b} \end{cases} \tag{2}$$

where a, b, d, and s are positive material constants, respectively.

In the first square bracket, the exponential function term is introduced to reflect the flow softening phenomenon caused by the microcracks under the large strain. The fourth term is used to describe the flow softening behavior induced by the temperature rise. And the hyperbolic tangent function is employed to describe the flow softening behavior induced by the temperature rise under the small strain.

Figure 1 compares the proposed MJC model with the J-C model. The parameters a and s are used to correct the drop slope of the stress-strain curve, which represent the degree of stress softening. Parameters D and P are introduced to describe effect of dynamic recrystallization and recovery mechanisms on flow stress. Parameters b and d are used to get the different levels of softening [1].

The inverse algorithm routine is shown in Fig. 2. The RSM based on the values of FE simulations is carried out to determine the correction parameters of the MJC constitutive model. Firstly, the four modified parameters are taken as design factors. And the cutting forces obtained from the FE simulations are taken as the response values. In RSM, CCD (central composite design) is widely used due to its flexibility and serviceability as sequential design of experiments. So, the CCD is adopted for the experiment design in this paper, as shown in Table 4. Parameters A, B, C, m, and n [25] are kept constants in order to preserve the flow stress at zero strain, the strain rate, and temperature effects compared to the original J-C model, respectively [31]. The parameter ranges come from the previous researches [1, 27]. Then, the FE simulations of orthogonal machining are conducted according to the CCD. Main cutting force and feed force can be obtained from the post-processor of Deform/2D. Thus, the response model between the cutting forces and the design factors is established using RSM. Based on the orthogonal cutting experiment, the process of determining the four modified parameters is taken as the parameter

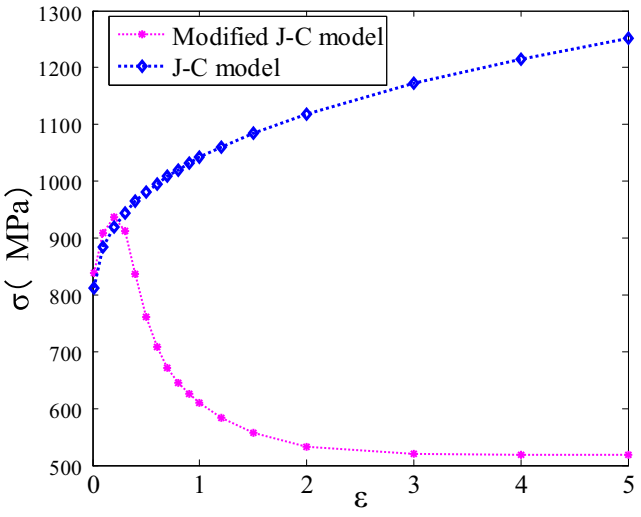

Fig. 1 Original and modified J-C model of titanium alloy Ti-6Al-4V ($A = 724.7$, $B = 683.1$, $C = 0.035$, $m = 1.0$, $n = 0.47$, $a = 3$, $b = 1$, $d = 1$, and $s = 2$)

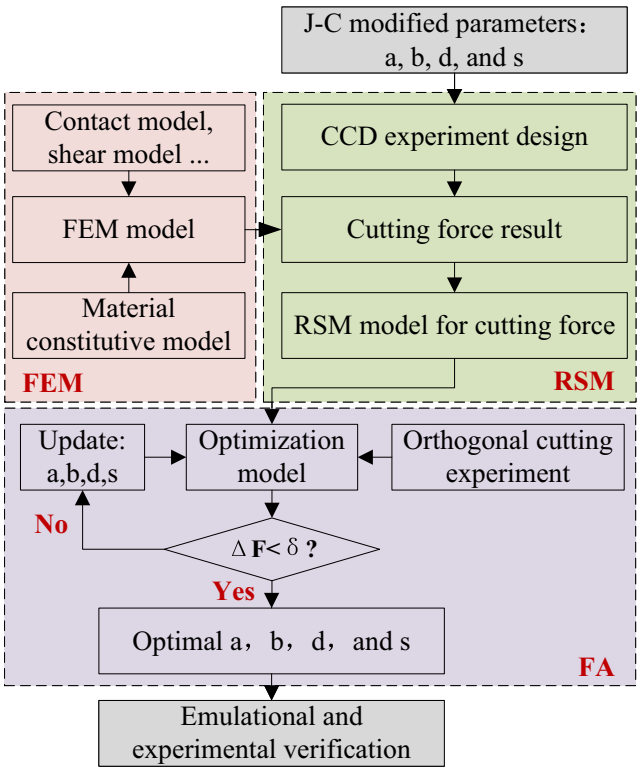

Fig. 2 Algorithm routine for determining added J-C coefficients

Table 1 Mechanical properties of titanium alloy Ti-6Al-4V

Tensile strength (MPa)	Yield strength (MPa)	Elastic modulus (GPa)	Expansion (m/m/k)	Density (kg/m^3)	Poisson's ratio
950	820	113.8	8.6e^{-6}	4430	0.342

optimization process. The FA is introduced to seek the optimal solution of modified parameters. Finally, cutting force experiments are conducted to verify the effectiveness of the proposed model.

3 Reverse analysis for added J-C coefficients of titanium alloy Ti-6Al-4V

3.1 Cutting force modeling

3.1.1 Finite element model of orthogonal cutting

The 2D finite element model (FEM) of orthogonal cutting titanium alloy Ti-6Al-4V is established on DEFORM-2D V10.2 platform. The workpiece of titanium alloy Ti-6Al-4V, rectangular block 4.5 mm × 1.05 mm × 0.10 mm, is defined as an elasto-plastic body. Its mechanical properties at room temperature are shown in Table 1. The workpiece is meshed with 5000 linear quadrilateral elements with four integration points. The uncoated carbide cemented carbide cutter is defined as a rigid body and meshed with 5000 linear quadrilateral elements with four integration points. The geometries of cutter are set as rake angle of 12.62°, relief angle of 7.36°, and edge radius of 30 μm, respectively. And temperature-dependent physical parameters of workpiece material are input into Deform/2D preprocessor as shown [31] in Table 2.

The constitutive data generated through the material identification process is used to model the flow stress behavior of the workpiece under the combined effect of strain, strain rate, and temperature. The parameters of the original J-C constitutive model A, B, C, n, and m are given in Table 3 [25].

Considering the adhesion of workpiece material to the cutter for machining titanium alloys, two contact models between cutter/chip interface, including coulomb contact model and shear contact model, are used to model the contact behavior. As shown in Eq. (3), the shear model is used for harsh contact conditions, while the coulomb model is used to describe slight contact behavior.

$$\begin{cases} m = \tau/k & \text{shear model} \\ \mu = \tau/\sigma_n & \text{coulomb model} \end{cases} \tag{3}$$

where τ is the shear stress, k is the shear flow stress of material, σ_n is the normal stress.

The friction between cutter and workpiece is defined by three spaced contact areas, as shown in Fig. 4. The shear friction coefficient used in the adhesive area from the tip to the tangent point of the workpiece and the cutter is set as 1. The shear friction coefficient is set as 0.85 from the tangent point to the uncut area. The remaining area of the rake face is very mild contacting with the chip, and the coulomb friction coefficient of the coulomb model with 0.5 is sufficient to describe the sliding contact.

The workpiece and cutter edges far from the cutting zone are retained at room temperature T_0 is 20 °C. The heat transfer coefficient h is set as 10^5 kW/m^2 °C to accelerate the temperature rise [32]. The thermal convection coefficient with the external environment is 0.02 W/m^2 k. Through mesh windows, a dense mesh is maintained in the cutting zone and in the newly generated surface. The workpiece consists of several areas with varying element edge size, ranging from 0.0025 mm at the top 10% of the workpiece and 0.0075 mm at between 10 and 30% of the workpiece to 0.07 mm at the rest. A similar approach is adopted for cutter, and elements are from 0.0167 mm near the tip to 0.125 mm at the rest in Fig. 3. An interference depth of 0.008 mm is implemented as an automatic remeshing criterion for the workpiece. Remeshing

Table 2 Thermal-mechanical properties of titanium alloy Ti-6Al-4V

Elastic modulus (E) (MPa)	α (mm/mm°C)	λ (W/m°C)	Cp (N/mm^2°C)
$0.7412\ T + 113{,}375$	$3 \times 10^{-9}\ T + 7 \times 10^{-6}$	$7.039e^{0.0011T}$	$2.24\ e^{0.0007T}$

Table 3 J-C model parameters

A (MPa)	B (MPa)	C	n	m	T_m (K)	T_r (K)	$\dot{\varepsilon}_0$ (s^{-1})
724.7	683.1	0.035	0.47	1.0	1877	293	10^{-5}

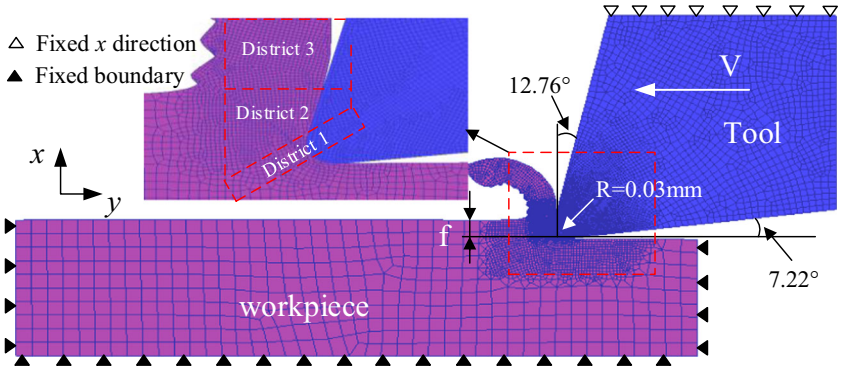

Fig. 3 FE model of orthogonal cutting

follows the defined mesh grading strategy throughout the simulation.

During the FE simulations, the cutting cutter moves relative to the fixed workpiece. The cutting width is set as 1 mm in default in Deform/2D. The feed rate (f) and cutting speed (v) are set as 0.10 mm/rev and 50 m/min, respectively. After reaching the desired stroke, cutting forces are then obtained from the post-processor (Fig. 4).

3.1.2 Response surface model of cutting force

In order to establish the relationship between added J-C parameters and cutting forces, an efficient experimental design method is needed. RSM includes the design of experiments, modeling, and the evaluation of relationship between controlled factors and optimum conditions. It is successfully applied in the optimization problems [33, 34]. Moreover, CCD of RSM can simultaneously analyze all levels and its simple calculation [35, 36]. In this work, four independent variables are researched at three levels in Table 4. And 28 experiments are screened to run as shown in Table 5. Then, insignificant ones are removed in order to obtain the more suitable factor combination. a, b, d, and s are selected as the design factors (independent variable X), denoted as X_1, X_2, X_3, X_4, respectively. The ranges of a, b, d, and s are selected according to the previous researches [1, 27]. The ranges are bounded in 0.01 and 6 as shown in Table 4. There is no need to expand the upper boundary of the parameters. Test factor codes and levels are also shown in Table 4. The relationships between the response values and the independent variables are fitted by third-order response surface equations, as shown in Eq. (4). Among Eqs. (5) and (6), F_X refers to the main cutting force F_c, which parallels to the Z direction of lathe. And F_Y refers to trust force F_t paralleling to the Z direction of lathe as introduced in Section 3.2.

$$\begin{aligned} Y = {} & \beta_0 + \sum_{i=1}^{4} \beta_{iii} x_i^3 + \sum_i \sum_j x_i^2 x_j + \sum_i \sum_j \beta_{ijj} x_i x_j^2 \\ & + \sum_i \sum_k \beta_{iik} x_i^2 x_k + \sum_i \sum_k \beta_{ikk} x_i x_k^2 \\ & \sum_j \sum_k \beta_{jjk} x_j^2 x_k + \sum_j \sum_k \beta_{jkk} x_j x_k^2 \\ & + \sum_i \sum_j \sum_{k(i \neq j \neq k)} \beta_{ijk} x_i x_j x_k + e\left(x_1, x_2, x_3, x_4,\right) \end{aligned} \tag{4}$$

where β_0 is constant term; x_i, x_j, and x_k are independent variables; β_{iii}, β_{iij}, β_{ijj}, β_{iik}, β_{ikk}, β_{jjk}, β_{jkk}, and β_{ijk} are regression coefficients of the one degree, two degree, three degree, and interaction items; and e is error. The experimental design

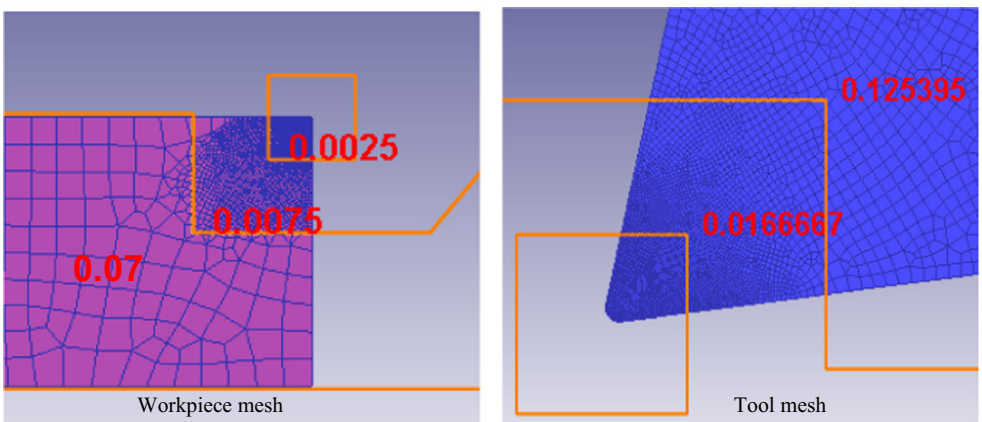

Fig. 4 Meshing scheme of workpiece and cutter

Table 4 Variables and their ranges

Factor codes	Name	Levels		
		− 1	0	+ 1
X_1	a	0.10	3.05	6.00
X_2	b	0.10	3.05	6.00
X_3	d	0.10	3.05	6.00
X_4	s	0.10	3.05	6.00

scheme generated by Design Expert V8.0 is shown in Table 5.

In order to guarantee the prediction accuracies of cutting force models, variance verifications of models are conducted by ANOVA as shown in Table 6. The computed F_X model F values of a (112.69), b (18.73), d (361.69), and s (0.69) imply that the F_X model is significant, and the chance of a model F value this large is only 0.01% due to noise from Table 7. The P value of F_X prediction model is lower than 0.0001. It indicates that this prediction model is extremely significant. The P value of lack of fit is 0.2565 (> 0.05). It indicates that the lack of fit of F_X prediction model is not significant. The correlation coefficient is $R^2 = 0.9976$ and adjustment coefficient is $\mathrm{Adj}R^2 = 0.9941$, which indicates F_X predictive model has a high degree of fitting. Therefore, it can effectively predict the cutting force of X direction. Similarly, the F value of F_Y prediction model is 144.06, $P < 0.0001$. The P value of lack of fit is 0.6114 (> 0.05). The correlation coefficient R^2 is 0.9953 and adjustment coefficient $\mathrm{Adj}R^2$ is 0.9883. It can be ensured that F_Y predictive model also has a high degree of fitting.

According to the reference [5] and factor significance analysis, non-significant items are deleted from the cubic polynomial equations as shown in Eqs. (5) and (6).

Table 5 Center compound design and simulated cutting forces

Order	a	b	d	s	F_X	F_Y
1	0.10	0.10	0.10	0.10	381.800	148.818
2	6.00	0.10	0.10	0.10	289.349	128.477
3	0.10	6.00	0.10	0.10	392.254	149.023
4	6.00	6.00	0.10	0.10	300.493	130.649
5	0.10	0.10	6.00	0.10	444.620	175.354
6	6.00	0.10	6.00	0.10	318.360	133.544
7	0.10	6.00	6.00	0.10	449.806	175.035
8	6.00	6.00	6.00	0.10	317.882	134.305
9	0.10	0.10	0.10	6.00	107.458	67.698
10	6.00	0.10	0.10	6.00	94.307	60.655
11	0.10	6.00	0.10	6.00	134.358	88.111
12	6.00	6.00	0.10	6.00	132.485	91.829
13	0.10	0.10	6.00	6.00	452.106	175.565
14	6.00	0.10	6.00	6.00	319.318	134.816
15	0.10	6.00	6.00	6.00	449.689	176.357
16	6.00	6.00	6.00	6.00	317.265	133.343
17	0.10	3.05	3.05	3.05	449.610	175.897
18	6.00	3.05	3.05	3.05	319.308	133.698
19	3.05	0.10	3.05	3.05	313.761	135.628
20	3.05	6.00	3.05	3.05	312.691	136.035
21	3.05	3.05	0.10	3.05	132.171	89.548
22	3.05	3.05	6.00	3.05	313.069	135.848
23	3.05	3.05	3.05	0.10	312.979	135.433
24	3.05	3.05	3.05	6.00	312.751	135.537
25	3.05	3.05	3.05	3.05	312.566	135.795
26	3.05	3.05	3.05	3.05	319.626	140.769
27	3.05	3.05	3.05	3.05	282.000	153.000
28	3.05	3.05	3.05	3.05	318.641	139.209

Table 6 Factor significance examination

	Independent variable	Standard error	F value	P value
F_X	X_1	1.56	112.69	< 0.0001
	X_2	1.56	18.73	0.0012
	X_3	4.69	361.69	< 0.0001
	X_4	4.69	0.69	0.4252
	X_1X_3	1.66	14.08	0.0032
	X_1X_4	1.66	6.22	0.0298
	X_2X_3	1.66	18.58	0.0012
	X_2X_4	1.66	7.99	0.0165
	X_3X_4	1.66	1018.14	< 0.0001
	X_1^2	3.95	71.72	< 0.0001
	X_3^2	3.95	349.15	< 0.0001
	X_4^2	3.95	8.73	0.0131
	$X_1X_3X_4$	1.66	6.00	0.0322
	$X_2X_3X_4$	1.66	7.25	0.0209
	$X_1^2X_3$	4.97	21.73	0.0007
	$X_1^2X_4$	4.97	99.41	< 0.0001
F_Y	X_1	0.62	205.84	< 0.0001
	X_2	1.86	0.29	0.6038
	X_3	0.62	872.89	< 0.0001
	X_4	1.86	0.33	0.5796
	X_1X_2	0.66	1.60	0.2320
	X_1X_3	0.66	48.78	< 0.0001
	X_1X_4	0.66	15.49	0.0023
	X_2X_3	0.66	57.84	< 0.0001
	X_2X_4	0.66	42.15	< 0.0001
	X_3X_4	0.66	424.50	< 0.0001
	X_1^2	1.43	63.32	< 0.0001
	X_3^2	1.43	106.11	< 0.0001
	$X_1X_3X_4$	0.66	8.09	0.0160
	$X_2X_3X_4$	0.66	38.84	< 0.0001
	$X_1^2X_2$	1.98	8.53	0.0139
	$X_1^2X_4$	1.98	40.45	< 0.0001

Table 7 Variance analysis of response surface model

	Sources of variation	Sum of squares	Degree of freedom	Mean value	*F* value	*P* value
F_X	Model	201,600	16	12,600.09	286.56	< 0.0001
	Residual	483.67	11	43.97		
	Lack of fit	417.81	8	52.23	2.38	0.2565
	Pure error	65.86	3	21.95		
	Total	202,100	27			
	$R^2 = 0.9976$, Adj$R^2 = 0.9941$					
F_Y	Model	15,995.76	16	999.73	144.06	< 0.0001
	Residual	76.34	11	6.94		
	Lack of fit	53.42	8	6.68	0.87	0.6114
	Pure error	22.91	3	7.64		
	Total	16,072.09	27			
	$R^2 = 0.9953$, Adj$R^2 = 0.9883$					

$$F_X = +363.99470 - 82.55987a + 1.53692b + 56.63997d + 5.27642ad + 12.73986as - 0.29063bd + 1.06887bs + 7.09114ds + 12.49094a^2 - 8.48471d^2 + 1.34146s^2 - 0.15820ads - 0.17391bds - 0.90305a^2d - 1.93151a^2s \quad (5)$$

$$F_Y = +143.87617 - 16.20602a + 13.01360d - 0.30597ad + 3.50607as - 0.087899bd + 0.97893bs - 2.26940ds + 2.11787a^2 - 1.69660d^2 - 0.072973ads - 0.15988bds + 0.22479a^2b - 0.48945a^2s \quad (6)$$

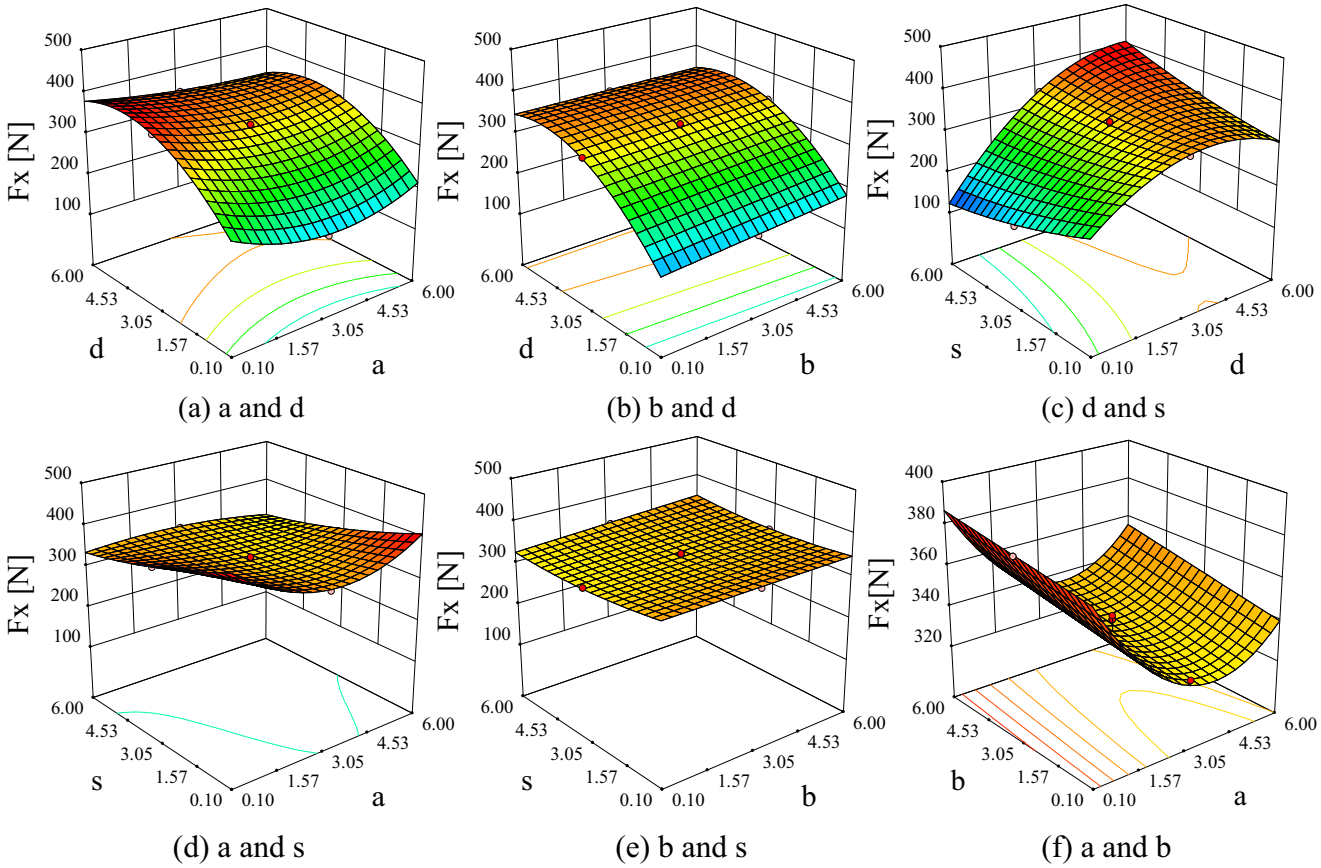

Fig. 5 Effect of added J-C coefficients on cutting force F_X

Figures 5 and 6 show the effect of added J-C coefficients on cutting forces F_X and F_Y, respectively. Figure 5(a, b) shows that the F_X value response was obtained from a and d and b and d, respectively. The decreasing effect of d on F_X can be justified by improving a, and thus decreasing the importance of d. Similarly, the decreasing effect of d on F_X can be justified by improving b. So, the optimum region to obtain the minimum F_X is at the upper limits of variables. Figure 5(c) shows the relation between the F_X value and parameters s and d. The increasing effect of s on F_X can be justified by decreasing d, and thus decreasing the importance of s. It can be inferred that the optimum area to obtain the minimum F_X is at the under limits of variables. Figure 5(d) shows that the increasing effect of a on F_X is decreased by improving s. Figure 5(e) shows that the coupling effect of b and s on F_X is negligible. From Figure 6(a), d shows positive effect on F_Y, a shows positive effect, then shows negative effect on F_Y. b shows negative effect on F_Y from Fig. 6(b). It can be obtained that from Fig. 6(d), s shows negative effect on F_Y. In Fig. 6(e), all variables show positive effect on F_Y. In Fig. 6(f), b shows positive effect on F_Y, while a shows negative effect at the beginning, then shows positive effect on F_Y. Obviously, d has the most significant effect in addition to b with slighter effect from Fig. 6.

3.2 Optimized process

3.2.1 Experiment procedure

The experiments of orthogonal cutting titanium alloy Ti-6Al-4V are conducted on HK63 CNC under dry cutting condition. The workpiece disk is obtained with cylindrical specimen with diameter of 160 mm and length of 70 mm. Sharp and coated cemented carbide inserts (SECO-LCMF-160404-0400-FT, CP500) are used, which are mounted on a left-hand holder. And the real working angles of cutter are determined from reference [37]. The working rake angle and the working relief angle are 12.62° and 7.36°. Additionally, a new cutting edge is employed to avoid the effect of cutter wear on cutting edge for each experiment.

The workpiece disk is pre-grooved to prefabricate convex plates with width of 2.0 mm for orthogonal cutting as shown in Fig. 7. The cutting force test system is consisted of Kistler force dynamometer (type 9255B), Kistler multichannel charge amplifier (type 5080A), dynamic data acquisition, processing system (Strtust STG), and data processing soft (DEWEsoftx7.1). The average cutting forces of stable cutting section are selected and calculated as the

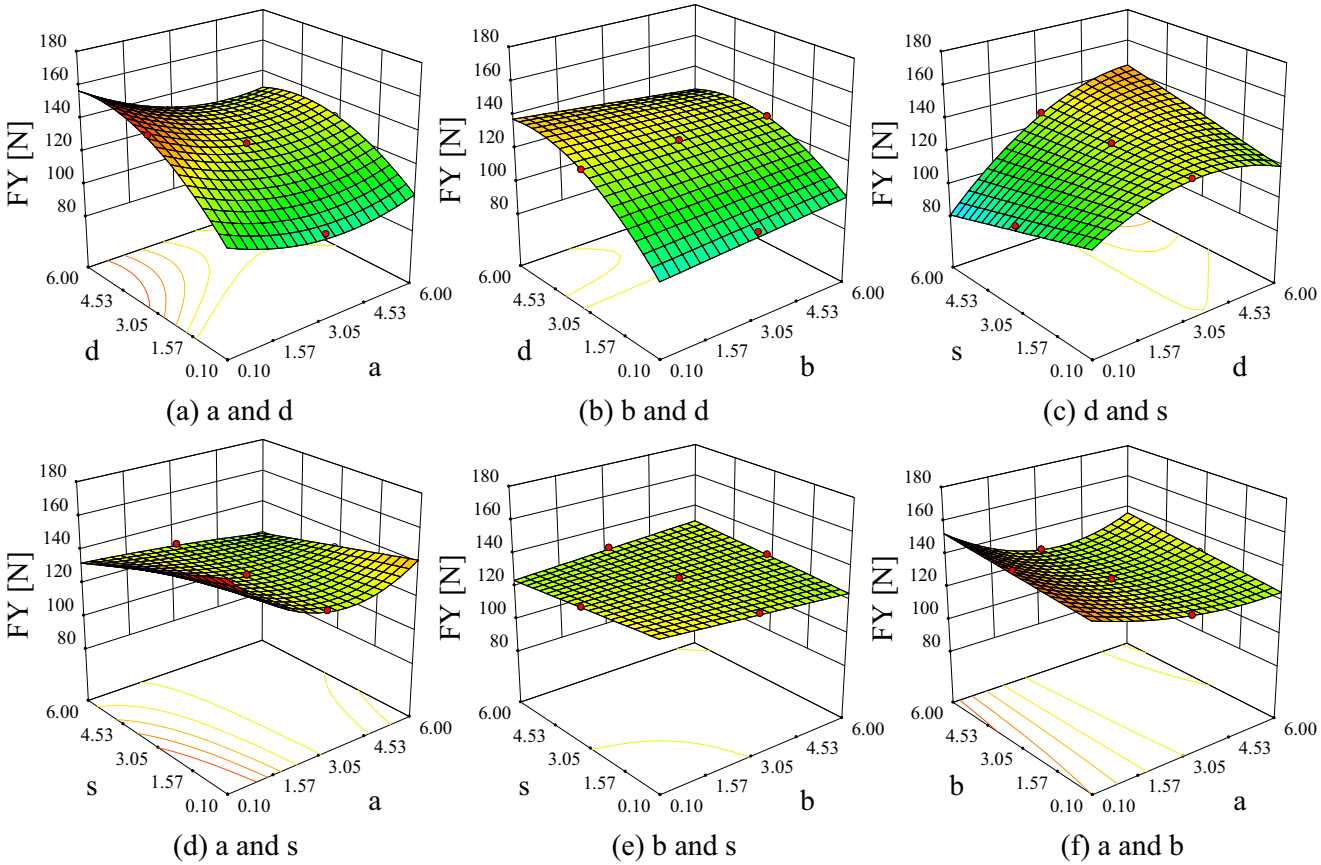

Fig. 6 Effect of added J-C coefficients on cutting force F_Y

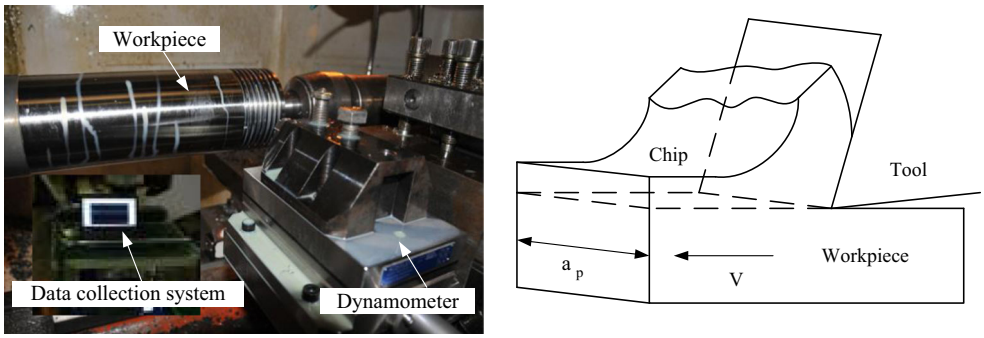

Fig. 7 Orthogonal cutting experiment

results for the inverse work and verification. And the average cutting force of three tests is taken as the final result.

The cutting speed is set as 50 m/min and the feed is 0.10 mm/rev. The measured main cutting forces F_X and feed force F_Y are 225.51 and 137.46 N, respectively. And the corresponding resultant force F_{Exp} is 264.10 N.

3.2.2 Optimized results

The optimization model is established with the cutting force prediction models and corresponding measured results as shown in Eq. (7).

$$\begin{aligned} &\text{Find}: (a,b,d,s)\\ &\text{Max}: \varepsilon = -\left|\left(F_X{}^2 + F_Y{}^2\right)^{0.5} - F_{Exp}\right|\\ &\text{Subject to}: \begin{cases} a_{\min} \le a \le a_{\max} \\ b_{\min} \le b \le b_{\max} \\ d_{\min} \le d \le d_{\max} \\ s_{\min} \le s \le s_{\max} \end{cases} \end{aligned} \tag{7}$$

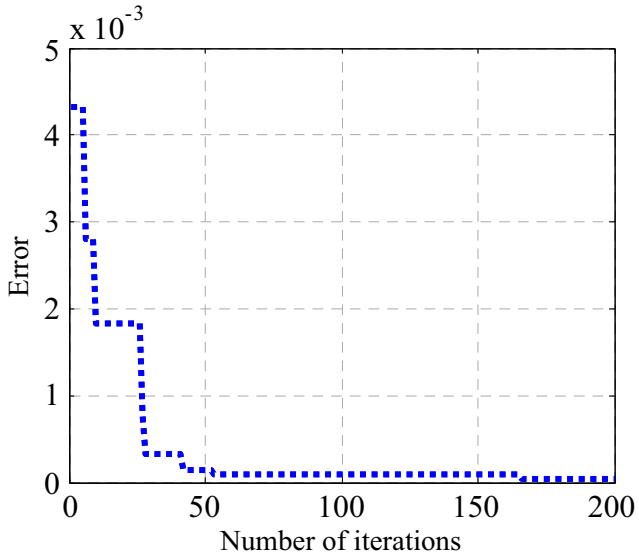

Fig. 8 Iteration process

After determining the optimization model based on the experimental resultant force F_{Exp}, FA is applied to obtain the optimal solution of modified parameters. FA, proposed by yang [38], is a nature-inspired metaheuristic algorithm based on a firefly's behavior. The main idea of flashes produced by a firefly is to attract mating partners. FA has been applied more and more extensively. Although it is similar to the Particle Swarm Optimization (PSO) and others' algorithms based on the swarm intelligence, it is simpler not only on concept but also implementation [39, 40]. And the most important thing is that FA is more efficient than other traditional algorithms, such as Genetic Algorithm (GA) [41].

In this paper, FA is adopted to search the optimal values of added J-C parameters. And the algorithm is performed on Matlab2012a platform with an Intel(R) Core(TM) i5-3450 CPU @ 3.10 GHz processor. In this optimization process, the set values of the control parameters are listed as follows. The number of fireflies is set as 500, which can better improve the effect of individual numbers on the decision domain. The light absorption coefficient γ is 1. The attraction of light β_0 is 1 (the maximum attraction constant). The initial fluorescein I_0 is 5. The step length is set to 0.05 and the maximum number of iteration is 200. The other input parameters are set as follows: density 4430 kg/m^3, specific heat 565 J/(kg k), coefficient of heat conduction between cutter and workpiece is 6.6 W/(m^2 k) [26], melting temperature 1877 K, reference temperature 297 K, reference strain rate 10^{-5} [42]. The original J-C parameters A, B, C, m, and n are given in Table 3. The termination error of the iterative process is 10^{-5}.

The optimization result is shown in Fig. 8. This optimization process confirmed that the FA has ability to achieve convergence rapidly with small error (2.11%). With the termination criterion defined by Eq. (7), the global optimum solution is found within 200 generations. Only 283.47 s is taken to accomplish the whole search process.

The optimization results are $a = 3.7758$, $b = 1.3247$, $d = 0.9076$, and $s = 2.6195$. Therefore, the modified J-C model of titanium alloy Ti-6Al-4V is given in Eq. (8).

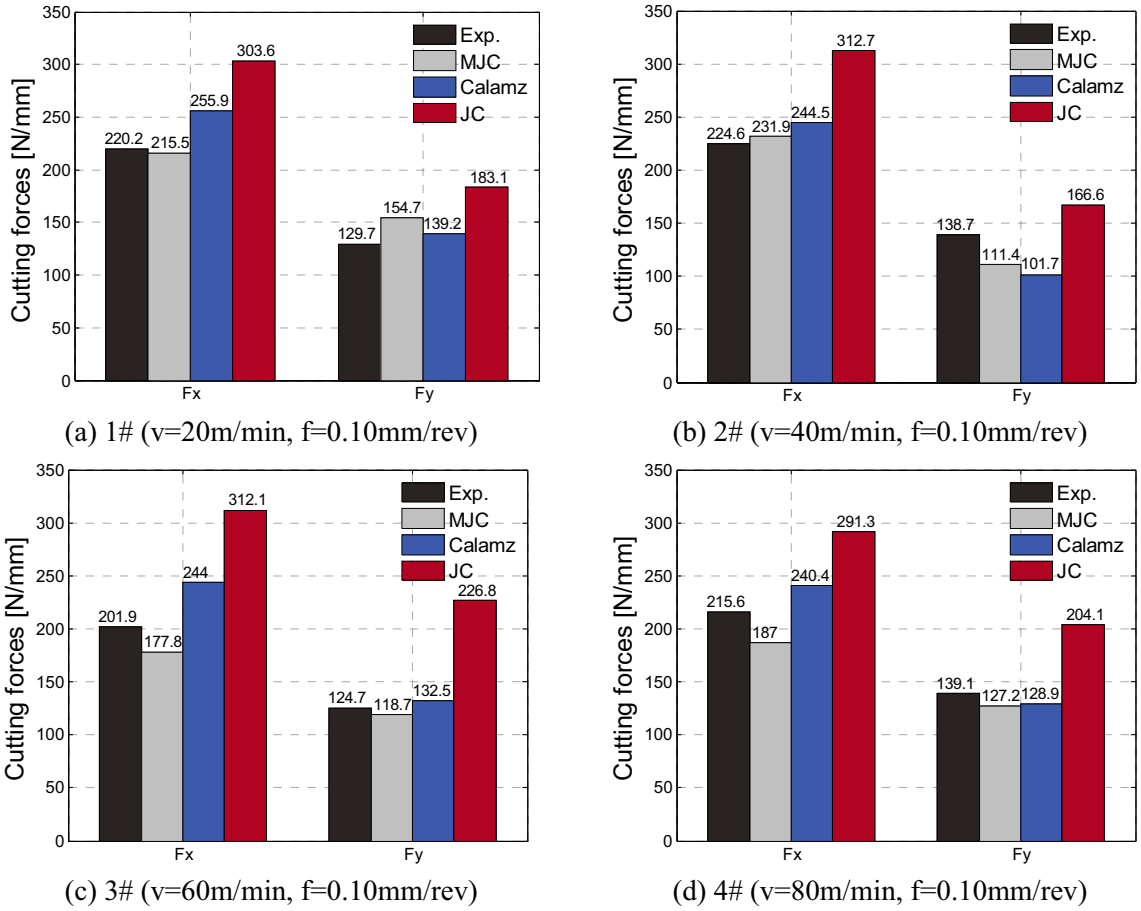

(a) 1# (v=20m/min, f=0.10mm/rev)

(b) 2# (v=40m/min, f=0.10mm/rev)

(c) 3# (v=60m/min, f=0.10mm/rev)

(d) 4# (v=80m/min, f=0.10mm/rev)

Fig. 9 Measured and simulated cutting forces

$$\begin{cases} \sigma = \left[724.7 + 683.1\varepsilon^{0.47}\left(\dfrac{1}{\exp(\varepsilon^{3.7758})}\right)\right]\left[1 + 0.035\ln\left(\dfrac{\dot{\varepsilon}}{10^{-5}}\right)\right]\left[1-\left(\dfrac{T-293}{1584}\right)\right]\left[D + (1-D)\left(\tanh\left(\dfrac{1}{\varepsilon + P}\right)\right)^{2.6195}\right] \\ D = 1-\left(\dfrac{T}{1877}\right)^{0.9076}, P = \left(\dfrac{T}{1877}\right)^{1.3247} \end{cases} \quad (8)$$

4 Verification

Four verification experiments are conducted to confirm the prediction accuracy of FEM with the proposed MJC model. The feed rate was fixed at 0.1 mm/rev when the cutting speed is set as 20, 40, 60, and 80 m/min, respectively. FE simulations with different constitutive models, including the proposed modified J-C model, Calamaz's model, and original J-C model, were performed on the software platform Deform2D 10.2. Meanwhile, orthogonal cutting experiments were carried out under the same cutting conditions.

The measured and simulated cutting forces are shown in Fig. 8. It can be obviously observed that the measured main cutting force changes from 201.9 to 224.6 N and the feed force ranges from 124.7 to 139.1 N. On the whole, the J-C model yields larger cutting forces while the modified J-C models have smaller values. The results show that the proposed MJC model has the highest prediction accuracy on cutting forces among the three constitutive models. The total average prediction error for the proposed MJC model, Calamz's model, and the J-C model is 10.38, 13.04, and 44.60%, respectively. The prediction error of the proposed MJC model is 10.74, 11.49, 8.35, and 10.90% in sequence for the four verification experiments. It indicates that the proposed constitutive model improves the prediction accuracy of FEM simulation. From Fig. 9 (a) and (b) it can be also found that the prediction error

of the proposed MJC model on main cutting force is smaller than that of feed force for the first two experiments. But the contrary is the case for the remaining two experiments, as shown in Fig. 9 (c) and (d). It indicates that there is a slight change on the prediction error with the increasement of cutting speed. That could be induced by adopting fixed friction coefficient for the FEM simulations and can be improved by using friction coefficient of velocity dependence. The consistency of cutting forces between experiments and simulations indicate the feasibility of the proposed inverse determination method of constitutive models of titanium alloy Ti-6Al-4V.

5 Conclusions

The origin J-C constitutive model often leads to deviation between finite element simulation and experiment. Modifying the J-C model by introducing hyperbolic tangent failure function is a promising way to improve the simulation precision of machining. The current work develops a new inverse procedure based on finite element analysis to identify the improved J-C model for machining titanium alloy Ti-6Al-4V. The variance analysis proves the effectiveness of the response surface method on relating the cutting forces with the added coefficients. A new modified J-C model of titanium alloy Ti-6Al-4V is subsequently obtained. Verification experiments demonstrate the effectiveness and advantages of the inverse identification method. A significant improvement is found on predicting cutting forces using FE simulation. This inverse approach could also be extended to other metal materials for cutting process.

Compliance with ethical standards

Conflicting of Interest The authors declare that they have no conflict of interest.

Appendix

Notation

a	Material constant
b	Material constant
d	Material constant
f	Feed
h	Heat transfer coefficient(kW/m^2°C)
m	Thermal softening factor
n	Hardening factor
r_s	Visible range of the firefly
s	Material constant
v	Cutting speed (m/min)
A	Yield strength (MPa)
B	Hardening modulus (MPa)
C	Strain rate sensitivity
$C_P(T)$	Heat capacity of workpiece (N/mm^{2}C)
$E(T)$	Young modulus of workpiece (MPa)
F_c	Main cutting force (N)
F_t	Feed force (N)
T	Temperature of workpiece material (k)
T_0	Reference temperature (°C)
T_m	Melting temperature of workpiece material (k)
T_r	Reference temperature (k)
X_i	Each firefly
Y_i	Fluorescein value
σ	Equivalent flow stress (MPa)
σ_n	Normal stress (MPa)
ε	Equivalent plastic strain
$\dot{\varepsilon}$	Equivalent strain rate (s^{-1})
$\dot{\varepsilon}_0$	Reference strain rate (s^{-1})
ρ	Workpiece density (kg/m^3)
α	Rake angle (rad)
$\alpha(T)$	Thermal expansion of workpiece (mm/mmC)
τ	Shear stress (MPa)
μ	Friction coefficient
λ	Ratio of inlet thickness to primary thickness
$\lambda(T)$	Thermal conductivity of workpiece (W/mC)
δ	Error
σ_n	Normal stress
τ	Shear stress
k	Shear flow stress of material
β_0	Constant term
γ	Light absorption coefficient

References

1. Calamaz M, Coupard D, Girot F (2008) A new material model for 2D numerical simulation of serrated chip formation when machining titanium alloy Ti-6Al-4V. Int J Mach Tools Manuf 48:275–288. https://doi.org/10.1016/j.ijmachtools.2007.10.014
2. Molinari A, Musquar C, Sutter G (2002) Adiabatic shear banding in high speed machining of Ti–6Al–4V: experiments and modeling. Int J Plast 18:443–459. https://doi.org/10.1016/S0749-6419(01)00003-1
3. Puls H, Klocke F, Veselovac D (2016) FEM-based prediction of heat partition in dry metal cutting of AISI 1045. Int J Adv Manuf Technol 86:737–745. https://doi.org/10.1007/s00170-015-8190-z
4. Johnson GR, Cook WH (1983) A constitutive model and data for metals subjected to large strains, high strain rates and high temperatures. 7th Int Symp Ballist 541–547. doi: https://doi.org/10.1038/nrm3209
5. Ulutan D, Özel T (2013) Determination of constitutive material model parameters in FE-based machining simulations of Ti-6Al-4V and in-100 alloys: an inverse methodology. Trans North Am Manuf Res Inst SME 41:368–373

6. Zerilli FJ, Armstrong RW (1987) Dislocation-mechanics-based constitutive relations for material dynamics calculations. J Appl Phys 61:1816–1825
7. Zerilli FJ, Armstrong RW (1996) Constitutive relations for titanium and Ti-6Al-4V. 370:315–318
8. Zerilli FJ, Armstrong RW (1998) Dislocation mechanics based constitutive equation incorporating dynamic recovery and applied to thermomechanical shear instability 429:215–218
9. Follansbee PS, Kocks UF (1988) A constitutive description of the deformation of copper based on the use of the mechanical threshold stress as an internal state variable. Acta Metall 36:81–93. https://doi.org/10.1016/0001-6160(88)90030-2
10. Chen G, Ren C, Yu W, Yang X, Zhang L (2012) Application of genetic algorithms for optimizing the Johnson-Cook constitutive model parameters when simulating the titanium alloy Ti-6Al-4V machining process. Proc Inst Mech Eng Part B J Eng Manuf 226:1287–1297. https://doi.org/10.1177/0954405412447735
11. Hou QY, Wang JT (2010) A modified Johnson-Cook constitutive model for Mg-Gd-Y alloy extended to a wide range of temperatures. Comput Mater Sci 50:147–152. https://doi.org/10.1016/j.commatsci.2010.07.018
12. Wang X, Huang C, Zou B, Liu H, Zhu H, Wang J (2013) Dynamic behavior and a modified Johnson–Cook constitutive model of Inconel 718 at high strain rate and elevated temperature. Mater Sci Eng A 580:385–390. https://doi.org/10.1016/j.msea.2013.05.062
13. Wang B, Liu Z (2015) Shear localization sensitivity analysis for Johnson–Cook constitutive parameters on serrated chips in high speed machining of Ti6Al4V. Simul Model Pract Theory 55:63–76. https://doi.org/10.1016/j.simpat.2015.03.011
14. Shokrieh MM, Kashani ARS, Mosalmani R (2016) A dynamic constitutive-micromechanical model to predict the strain rate-dependent mechanical behavior of carbon nanofiber/epoxy nanocomposites. Iran Polym J (English Ed) 25:487–501. https://doi.org/10.1007/s13726-016-0441-9
15. Liu R, Melkote S, Pucha R, Morehouse J, Man X, Marusich T (2013) An enhanced constitutive material model for machining of Ti-6Al-4V alloy. J Mater Process Technol 213:2238–2246. https://doi.org/10.1016/j.jmatprotec.2013.06.015
16. Nemat-Nasser S, Guo WG, Nesterenko VF, Indrakanti SS, Gu YB (2001) Dynamic response of conventional and hot isostatically pressed Ti-6Al-4V alloys: experiments and modeling. Mech Mater 33:425–439. https://doi.org/10.1016/S0167-6636(01)00063-1
17. Liu L, Ming L, Wu W (2014) Recrystallization softening effect in the improved constitutive equation for TI-6AL-4V alloy. Rare Met Mater Eng 43:1367–1371
18. LIU Lijuanl, LU Min91, WU Wenge2 An improved constitutive model and finite element simulation for machining Ti-6Al-4V alloy
19. Rittel D, Landau P, Venkert A (2008) Dynamic recrystallization as a potential cause for adiabatic shear failure. Phys Rev Lett 101:165501
20. Ding R, Guo ZX (2004) Microstructural evolution of a Ti–6Al–4V alloy during β-phase processing: experimental and simulative investigations. Mater Sci Eng A 365:172–179
21. Ding R, Guo ZX, Wilson A (2002) Microstructural evolution of a Ti–6Al–4V alloy during thermomechanical processing. Mater Sci Eng A 327:233–245
22. Miller RM, Bieler TR, Semiatin SL (1999) Flow softening during hot working of Ti-6Al-4V with a lamellar colony microstructure. Scr Mater 40:1387–1393
23. Sima M, Özel T (2010) Modified material constitutive models for serrated chip formation simulations and experimental validation in machining of titanium alloy Ti-6Al-4V. Int J Mach Tools Manuf 50:943–960. https://doi.org/10.1016/j.ijmachtools.2010.08.004
24. Xue Q, Meyers MA, Nesterenko VF (2002) Self-organization of shear bands in titanium and Ti–6Al–4V alloy. Acta Mater 50:575–596
25. Calamaz M, Coupard D, Girot F (2017). Numerical simulation of titanium alloy dry machining with a train softening constitutive law numerical simulation of titanium alloy. doi: https://doi.org/10.1080/10910344.2010.500957
26. Calamaz M, Coupard D, Nouari M, Girot F (2011) Numerical analysis of chip formation and shear localisation processes in machining the Ti-6Al-4V titanium alloy. Int J Adv Manuf Technol 52:887–895. https://doi.org/10.1007/s00170-010-2789-x
27. Karpat Y (2015) A modified material model for the finite element simulation of machining titanium alloy Ti-6Al-4V. Mach Sci Technol An Int J 344:37–41. https://doi.org/10.1080/10910344.2010.512499
28. Andrade U, Meyers MA, Vecchio KS, Chokshi AH (1994) Dynamic recrystallization in high-strain, high-strain-rate plastic deformation of copper. Acta Metall Mater 42:3183–3195. https://doi.org/10.1016/0956-7151(94)90417-0
29. Yong Y, Wei-wei ZHU, Ming LI (2014) Construction of material constitutive model during cutting process for aeronautical titanium alloy based on orthogonal cutting Theory 24:
30. Bäker M, Rösler J, Siemers C (2002) A finite element model of high speed metal cutting with adiabatic shearing. Comput Struct 80:495–513. https://doi.org/10.1016/S0045-7949(02)00023-8
31. Pan Z, Liang SY, Garmestani H, Shih DS (2016) Prediction of machining-induced phase transformation and grain growth of Ti-6Al-4 V alloy. Int J Adv Manuf Technol 87:859–866. https://doi.org/10.1007/s00170-016-8497-4
32. Abboud E, Shi B, Attia H, et al (2013) Finite element-based modeling of machining-induced residual stresses in Ti-6Al-4V under finish turning conditions. Procedia CIRP8:63–68. doi: https://doi.org/10.1016/j.procir.2013.06.066
33. Ramesh S, Muthuvelayudham R, Rajesh KR, Viruthagiri T (2013) Enhanced production of xylitol from corncob by Pachysolen tannophilus using response surface methodology. Int J Food Sci 2013(514676):1–8
34. Malahat R, Mahiran B, Bakar SA et al (2014) Formulation development and optimization of palm kernel oil esters-based nanoemulsions containing sodium diclofenac. Int J Nanomed 9:539
35. Bezerra MA, Santelli RE, Oliveira EP, Villar LS, Escaleira LA (2008) Response surface methodology (RSM) as a tool for optimization in analytical chemistry. Talanta 76:965–977
36. Kasim MS, Che HCH, Ghani JA, Sulaiman MA (2013) Prediction surface roughness in high-speed milling of Inconel 718 under MQL using RSM method. Middle East J Sci Res 13:264–272
37. Zhou J, Ren J, Feng Y, Tian W, Shi K (2017) A modified parallel-sided shear zone model for determining material constitutive law. Int J Adv Manuf Technol 91:589–603. https://doi.org/10.1007/s00170-016-9717-7
38. Bäker M (2006) Finite element simulation of high-speed cutting forces. J Mater Process Technol 176:117–126. https://doi.org/10.1016/j.jmatprotec.2006.02.019
39. Yang XS (2010) Firefly algorithm, Lévy flights and global optimization. 20:209–218
40. Yang XS (2010) Firefly algorithm, stochastic test functions and design optimisation. Int J Bio-Inspired Comput 2:78–84(7)
41. Apostolopoulos T, Vlachos A (2011) Application of the firefly algorithm for solving the. doi: https://doi.org/10.1155/2011/523806
42. Lalwani DI, Mehta NK, Jain PK (2009) Extension of Oxley's predictive machining theory for Johnson and Cook flow stress model. J Mater Process Technol 209:5305–5312